



Contents lists available at ScienceDirect

Atmospheric Environment

journal homepage: www.elsevier.com/locate/atmosenv

Applications of optical spectroscopy and stable isotope analyses to organic aerosol source discrimination in an urban area

N. Mladenov^{a,*}, L. Alados-Arboledas^{b,c}, F.J. Olmo^{b,c}, H. Lyamani^b, A. Delgado^d, A. Molina^c, I. Reche^a^aDepartamento de Ecología, Universidad de Granada, 18071-Granada, Spain^bCentro Andaluz de Medio Ambiente-CEAMA, Av. del Mediterráneo s/n, 18006-Granada, Spain^cDepartamento de Física Aplicada, Universidad de Granada, 18071-Granada, Spain^dInstituto Andaluz de Ciencias de la Tierra (CSIC), 18100 Armilla, Granada, Spain

ARTICLE INFO

Article history:

Received 8 July 2010

Received in revised form

11 January 2011

Accepted 12 January 2011

Keywords:

Fluorescence

Absorbance

PARAFAC

Diesel

Sun photometry

African dust

ABSTRACT

Understanding the chemical character of organic aerosols is extremely important for evaluating their role in climate forcing and human respiratory health. Aerosol columnar properties retrieved by sun photometry represent a large dataset of information about the physical and light absorbing and scattering properties of the total aerosol, but lack more detailed chemical information about the organic fraction of atmospheric particulate matter. To obtain additional information about relationships between organic aerosol sources and columnar properties, we simultaneously examined stable isotope properties of PM₁₀ aerosols from urban (Granada, Spain) and remote (Sierra Nevada, Spain) sites and diesel exhaust, spectroscopic properties of water soluble organic carbon (WSOC) of PM₁₀ aerosols, and sun photometry measurements. We demonstrated that C and N stable isotopes and parameters from UV–vis and fluorescence spectroscopy are able to discriminate between aerosols receiving substantial fossil fuel pollution and those influenced by Saharan dust in an urban area. More depleted $\delta^{13}\text{C}$ was associated with low asymmetry parameter, g_{λ} , and high values of the spectral slope ratio, S_R , were associated with high effective radius, typical of pollution situations. The humification index (HIX), used predominantly to evaluate the degree of organic matter humification, was significantly related to g_{λ} and the radius of fine mode particles, r_f , and may reflect aging of the Saharan dust-influenced aerosols. Parallel factor analysis (PARAFAC) modeling identified a fluorescent component (C3) with a spectrum similar to that of naphthalene, which was significantly related to g_{λ} and r_f . The diesel exhaust sample represented a pollution end-member, with the lightest $\delta^{13}\text{C}$ value (-26.4‰), lowest S_R (0.95), lowest HIX (2.77) and highest %C3 (20%) of all samples.

© 2011 Elsevier Ltd. All rights reserved.

1. Introduction

There is substantial interest in tracking organic aerosols and understanding their chemical quality due to their effects on visibility, human respiratory health, and climate change (Jacobson et al., 2000). The organic chemicals in diesel exhaust include quinones, nitroaromatic hydrocarbons, aldehydes, aliphatic hydrocarbons, and polyaromatic hydrocarbons (PAHs), such as naphthalene (Baeza-Squiban et al., 1999). Soluble diesel exhaust particles have been shown to induce inflammation in bronchial epithelial cells (Baeza-Squiban et al., 1999), which can lead to numerous respiratory conditions. In particular, redox active quinones have been implicated

in the production of reactive oxygen species that produce oxidative stress and damage to airway epithelial cells (Baeza-Squiban et al., 1999; Cho et al., 2004).

Saharan- and north African-derived dust aerosols are responsible for more than half of the world's aerosol load (Washington et al., 2003; Schütz et al., 1981), depositing between 6 and 16 g m⁻² yr⁻¹ at a high elevation site in southern Spain (Morales-Baquero et al., 2006; Mladenov et al., 2009) and equally large amounts in Italy (Perrino et al., 2009) and elsewhere in the Mediterranean region. Estimates of organic carbon in Saharan dust include 10% (Maria et al., 2004) and 15% (Mladenov et al., 2010) and Saharan dust is an important source of organic matter for remote areas of southern Spain (Mladenov et al., 2008, 2009, 2010). Saharan dust outbreaks have been linked to human health and mortality in Spain (Perez et al., 2008). Given the recent rise in dust outbreaks and expectations that frequency, intensity, and distribution of these events will continue to increase (Prospero and Lamb, 2003), it is extremely important

* Corresponding author. Present address: INSTAAR, 450 UCB, University of Colorado, Boulder, CO 80309-0450, USA. Tel.: +1 720 233 2007; fax: +1 303 492 6388.
E-mail address: mladenov@colorado.edu (N. Mladenov).

to understand the chemical character of desert dust aerosols and be able to differentiate them from urban pollution aerosols.

Recently, optical spectroscopic techniques have been used to track organic aerosol deposition to lakes (Mladenov et al., 2009) and provide information about the chemical character of water soluble organic carbon (WSOC) in organic aerosols (Mladenov et al., 2010; Duarte et al., 2004, 2005) and wet deposition (Mladenov et al., 2010; Muller et al., 2008; Kieber et al., 2006). In particular, the use of UV–visible (UV–vis) absorbance and fluorescence techniques provides a vast amount of information about the provenance of bulk organic material that is not hindered by the sample volume, processing, and time requirements of more detailed chemical procedures, such as gas chromatography and liquid chromatography mass spectroscopy. UV–vis absorption provides important information about the presence of chromophoric compounds (Andreae and Gelencser, 2006; Sun et al., 2007; Morris et al., 1995) and aromatic structures (Weishaar et al., 2003). Some fulvic and humic-like substances (HULIS) and other light absorbing organic compounds, known collectively as brown carbon (C_{brown}) (Andreae and Gelencser, 2006), also emit fluorescence when excited by UV and visible light. Fluorescence spectroscopy provides information about organic matter sources and transformations, and its use to characterize WSOC (Duarte et al., 2005) and monitor aerosols *in situ* (Pinnick et al., 2004) is increasing. Parallel factor analysis (PARAFAC) modeling has recently been used in the study of aquatic organic matter to quantify dominant fluorescent components (Stedmon et al., 2003), but it has not yet been applied in the study of WSOC fluorescence. Stable isotopes of C and N also have been used extensively for DOM source characterization, and their use in aerosol characterization is on the rise (Widory, 2007; Schefub et al., 2003; Cachier, 1989).

Recent work has shown that the spectroscopic properties of organic aerosol deposition at a high mountain site were consistent with columnar properties of the total aerosol, such as aerosol optical depth and volume concentration of coarse particles (Mladenov et al., 2010). Three-dimensional fluorescence spectra of WSOC in Saharan-derived aerosol deposition collected at the same remote site were also found to be distinct from those of marine-derived aerosol WSOC (Mladenov et al., 2009). In contrast, little is known about the spectroscopic or stable isotopic signatures of organic aerosols in urban areas that are subject to both Saharan dust deposition and fossil fuel emissions.

Our goals in this study were: 1) to evaluate whether spectroscopic and stable isotopic signatures and commonly used absorbance and fluorescence indices supported the characterization of PM_{10} urban aerosols by ground based remote sensing, and 2) to identify distinguishing features of Saharan dust- and pollution-derived aerosols using optical spectroscopic and stable isotopic techniques.

2. Abbreviated methods

2.1. PM_{10} aerosol sampling and analyses

PM_{10} aerosol samples were collected from a rooftop monitoring station at the Andalusian Environmental Center in Granada (CEAMA), Spain weekly (one 24 h sampling per week) during the summer of 2008 and on two dates (48 h sampling each) at the remote observatory at the Sierra Nevada monitoring station. Samples were collected on pre-combusted quartz and glass fiber filters by means of a high volume PM_{10} sampler MCV PM1025 (model CAV-A/MS) operated at an average flow rate of $30 \text{ m}^3 \text{ h}^{-1}$. Because of the importance of particulate emissions from mobile sources, such as diesel exhaust, for air pollution in European cities, we also sampled PM_{10} aerosols of diesel exhaust from a light-duty

diesel truck run simultaneously in an enclosure with the PM1025 sampler. Potential sampling artefacts due to adsorption or volatilization of carbonaceous species during aerosol sampling should be addressed when considering the WSOC air concentration and WSOC spectroscopic character in an urban setting (Viana et al., 2006; Jacobson et al., 2000). To evaluate potential adsorption artefacts under ambient conditions, we deployed a “control” filter in an inoperative PM1025 sampler positioned alongside the CEAMA PM1025 sampler.

2.1.1. Total carbon, total organic carbon, and total nitrogen content

Total carbon (TC) content and total nitrogen (TN) content of a 1/8 portion of each CEAMA filter, a 1/16 portion of each diesel experiment filter, and a 1/4 portion of each Sierra Nevada filter were measured using a Carlo Elba NC1500 elemental analyzer on line with a Delta Plus XL mass spectrometer (EA-IRMS). The organic carbon (OC) content was measured after samples were exposed to concentrate HCl to eliminate carbonates. Due to potential incomplete removal of elemental carbon (EC), the OC measurements for the urban samples of this study, where EC is expected to be high, may be biased toward higher values.

2.1.2. Stable isotopes analyses of PM_{10} filters

Analyses of nitrogen and carbon isotopic composition were performed using a Carlo Elba NC1500 elemental analyzer on line with a Delta Plus XL mass spectrometer (EA-IRMS) with internal standards for carbon and nitrogen. The stable isotope composition is reported as δ values per mil: $\delta = (R_{\text{sample}}/R_{\text{standard}} - 1) * 1000$ where $R = {}^{13}\text{C}/{}^{12}\text{C}$ for $\delta^{13}\text{C}$ values and $R = {}^{15}\text{N}/{}^{14}\text{N}$ for $\delta^{15}\text{N}$.

2.2. Water soluble organic compound analyses

2.2.1. WSOC extraction

Water soluble organic compounds were extracted from the PM_{10} filters by agitating filter portions with purified water. To compare the influence of extraction methods on fluorescence properties, samples from the diesel exhaust experiments were extracted in duplicate via two commonly used methods, 1) mechanical shaking for 20 min and 2) sonication for 20 min in an ice bath.

2.2.2. DOC concentration

DOC concentrations were measured on acidified (with HCl) aqueous WSOC extracts from portions of each Granada, Sierra Nevada, and diesel experiment filters (Supplementary Materials). DOC concentration was measured in duplicate with a Shimadzu TOC-V CSH total organic carbon analyzer. WSOC air concentration was determined by multiplying DOC concentration by the extraction volume and normalizing to the volume of aerosol represented by each filter portion.

2.2.3. UV–vis absorbance measurements

UV–vis absorbance scans were measured in duplicate using a Perkin Elmer Lambda 40 spectrophotometer. After blank subtraction, absorbance at 250 nm and 320 nm was expressed as the Napierian absorption coefficient (a_{250} and a_{320}) corrected for the volume of air filtered and the volume of extractant used. The molar absorption coefficient (ϵ) ($\text{m}^2 \text{ mol}^{-1}$) was calculated by dividing the absorption coefficient at wavelengths of interest by the DOC concentration in mmol L^{-1} . The spectral slope from 275 to 295 nm and slope ratio (S_R) were calculated according to Helms et al. (2008).

2.2.4. Fluorescence spectral acquisition

Excitation emission matrices (EEMs) are a 3-dimensional representation of fluorescence intensities scanned over a range of

excitation:emission (ex/em) wavelengths. EEMs were measured using a JY-Horiba Spex Fluoromax-4 spectrophotometer. Instrument-specific corrections, Raman normalization, inner-filter correction, and blank subtraction were performed (Supplementary Materials). The EEM of the filtrate extracted from the blank filter was subtracted from each sample EEM. The fluorescence index (FI) and humification index (HIX) were calculated according to Cory and McKnight (2005) and Zsolnay et al. (1998), respectively.

2.2.5. PARAFAC modeling

EEMs of the Granada WSOC were modeled with PARAFAC according to Stedmon and Bro (2008) using the DOMFluor toolbox. Diesel experiment samples were subsequently fit to the PARAFAC model with residual EEM intensities representing <10% of measured EEM intensities. The fluorescence intensity was calculated on a molar basis for each component ($fC1$, $fC2$, and $fC3$) (Mladenov et al., 2009) and the percentage of total DOM fluorescence was also calculated for each component.

2.3. Ground-based remote sensing parameters

Measurements for atmospheric columnar characterization of the aerosol load were obtained using a Cimel CE-318 sun-photometer mounted on the roof of the CEAMA building, near the PM_{10} collector, and instrument-specific settings are described in detail in Holben et al. (1998) and Lyamani et al. (2006a,b).

Direct irradiance measurements at 340, 380, 440, 670, 870, 940, and 1020 nm were used to compute the aerosol optical depth, $\delta_{A\lambda}$, (dimensionless), at each wavelength except for the 940 nm channel, which is used to retrieve total column water vapour. For the retrieval of $\delta_{A\lambda}$ we first removed cloud-contaminated measurements (Smirnov et al., 2000). The $\delta_{A\lambda}$ is derived from the total optical depth obtained from direct sun-photometer measurements data using the appropriate calibration constant and subtracting the Rayleigh optical depth as well as the O_3 and NO_2 absorption optical depths (Alados-Arboledas et al., 2003; Lyamani et al., 2005, 2006b). For ozone content we used values measured by the Ozone Monitoring Instrument (OMI) (http://toms.gsfc.nasa.gov/ozone/ozone_v8.html). The NO_2 column contents were obtained from midlatitude model atmospheres in the LOWTRAN7 code (Kneizys et al., 1988). A ratio of $\delta_{A440}:\delta_{A1020}$ was developed, and, based on the results of Lyamani et al. (2006b), this ratio is close to 1.0 for Saharan dust-dominated days and >1.0 for high pollution conditions.

The Angström wavelength exponent, α (dimensionless) was computed from $\delta_{A\lambda}$ data assuming the model proposed by Angström, described in Lyamani et al., (2006b). Large values of α indicate the prevalence of fine particles from urban-industrial and biomass burning sources, while low values of α are related with the presence of coarse particles, such as desert dust and marine aerosols (Lyamani et al., 2006b).

The sky radiance almucantar measurements at 440, 670, 870, and 1020 nm, in conjunction with aerosol optical depth measurements at these same wavelengths, were utilized to retrieve the aerosol size distribution (including volume (V_f , V_c) and radii (r_f , r_c) of fine and coarse mode particles, respectively), the single scattering albedo, $\omega_{0A\lambda}$, and the asymmetry parameter, g_λ , based on the method of Nakajima et al. (1996) using the non-spherical approach proposed by Olmo et al. (2006, 2008). In this method the refractive index is invariant with wavelength. These parameters were derived by iteration, minimizing the residuals between measured and calculated radiances.

PM_{10} aerosols were characterized as Saharan-influenced (S) or Euro-dominated (E) based on their columnar properties and air mass backward trajectories. Daily backward trajectories (<http://www.arl.noaa.gov/ready.html>) were computed for Granada, Spain using the

HYSPLIT model (Draxler and Rolph, 2003) with archived data from the Global Data Assimilation System (GDAS) dataset and 120 h run time. Backward trajectories from 500 m above ground level (a.g.l.) were consulted for each day of sampling, and representative trajectories are shown for Saharan-influenced and Euro-dominated periods (Fig. 1a and b). For the Granada urban setting (Fig. 1b), Mladenov et al. (2010) determined from LIDAR imagery that the high concentration of Granada urban aerosols masked both the spectroscopic signatures and columnar properties of marine aerosols. More detailed methods are available in the Supplementary Materials that accompany this paper.

3. Results

3.1. C and N content and stable isotopes of PM_{10}

TC air concentrations of urban samples ranged from 2.04 to 10.61 $\mu\text{g C m}^{-3}$. OC concentrations ranged from 1.48 to 2.92 $\mu\text{g C m}^{-3}$ and represented approximately 52% \pm 14% of the TC (Table 1). TN concentrations ranged from 0.64 to 1.45 $\mu\text{g N m}^{-3}$ (Table 1). For remote samples from the Sierra Nevada, TC, OC, and TN air concentrations were substantially lower than for urban samples (Table 1).

In terms of their $\delta^{13}\text{C}$ and $\delta^{15}\text{N}$, samples from days with Saharan-influenced air masses plotted close to the remote Sierra Nevada samples, whereas samples from Euro-dominated days plotted close to the diesel sample (Fig. 2). In general, Saharan-influenced and Euro-dominated days had similar $\delta^{13}\text{C}$ values (mean of -26.2‰ for both) (Table 1). The diesel exhaust sample had the lightest $\delta^{13}\text{C}$ and $\delta^{13}\text{C}$ values at -26.4‰ and -25.4‰ , respectively, and a $\delta^{15}\text{N}$ value of 8.95‰. Saharan-influenced days had substantially lighter $\delta^{15}\text{N}$ values (mean 8.4‰) than Euro-dominated days (mean 10.2‰) (Table 1).

3.2. WSOC air concentrations and spectroscopic properties

WSOC air concentrations in urban samples ranged from 1.67 to 2.38 $\mu\text{g C m}^{-3}$ and were substantially higher than for remote Sierra Nevada samples (Table 2). UV–vis molar absorption at 250 nm and 320 nm in urban samples ranged from 46 to 60 and 20–29 $\text{m}^2 \text{mmol}^{-1}$, respectively (Table 2). The spectral slope ($S_{275-295}$) and slope ratio ranged from 0.008 to 0.011 nm^{-1} and 1.12 to 1.52, respectively. S_R values from the diesel experiment were substantially lower than urban samples (Table 2). The absorption signature of the control filter was negligible after blank subtraction (Table 2).

EEM spectra of Saharan-influenced and Euro-dominated WSOC (representative EEMs are shown in Fig. 1a and b) had a broad peak at an excitation of 240 nm that extended from 340 nm to 500 nm emission and another prominent peak extending from 290 to 320 nm excitation and 380–420 nm emission. In WSOC samples from Euro-dominated days (Fig. 1b), another peak was also visible at ex/em of 270/330–350 nm and the peak at 240 nm excitation was broadened. The peak at 270 nm excitation was also present in EEMs of WSOC from the diesel experiment along with a broadened peak at 240 nm excitation and dual peaks at approximately 290 nm and 340 nm excitation and 400 nm emission. The FI ranged from 1.48 to 1.64 (Table 3). HIX values for Granada urban WSOC ranged from 2.79 to 4.89 and, with the exception of the 23 June and 12 July 2008 samples, were generally higher in Saharan dust-derived WSOC (Table 3). HIX values for diesel experiment samples were between 1.91 and 2.84 depending on the treatment employed (Table 3). The fluorescence signature of the control filter was negligible after blank subtraction with no fluorescence intensity exceeding 0.1 RU (Supplementary Materials, Figure S2).

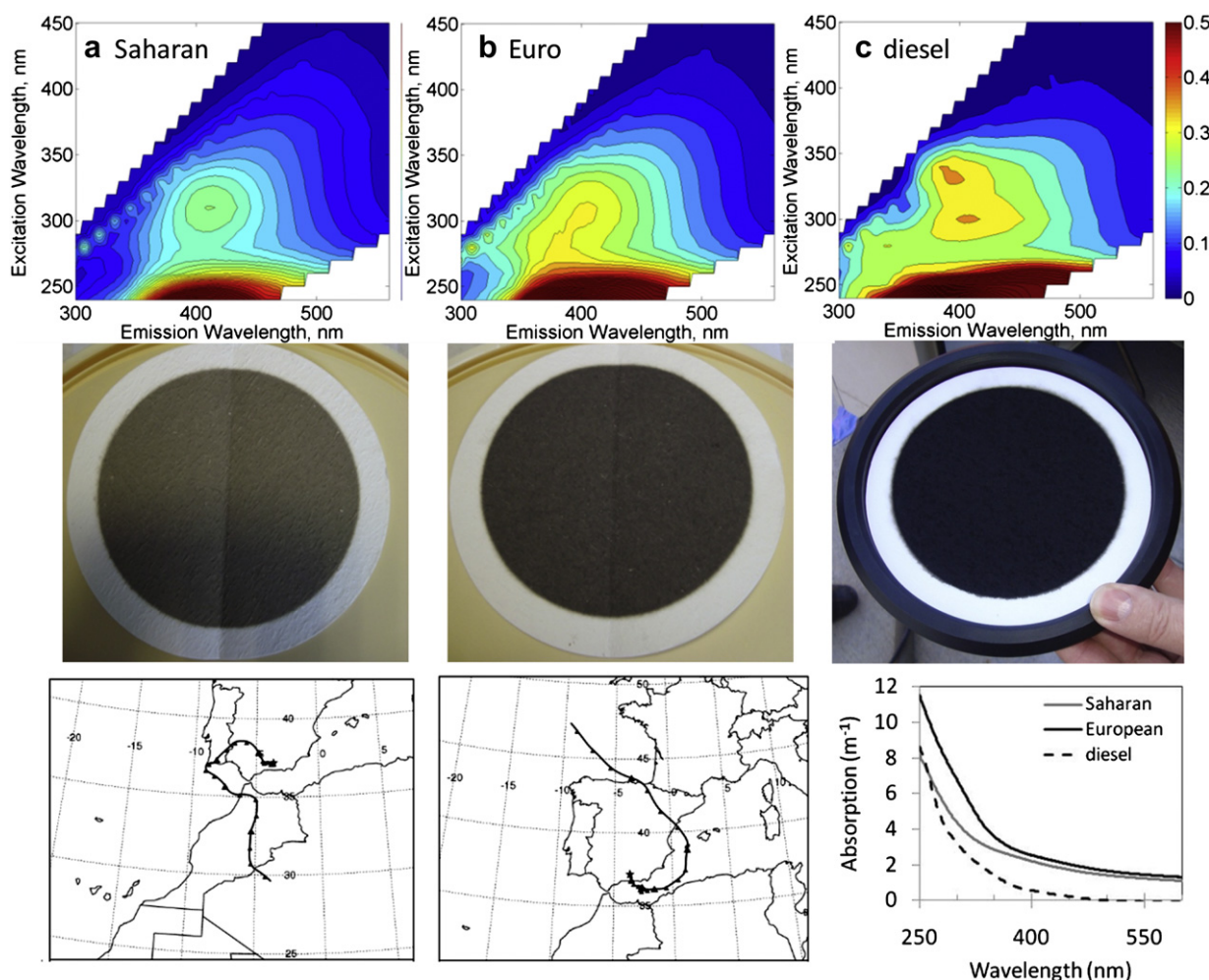


Fig. 1. Representative three-dimensional excitation emission matrices (EEMs; top panel) of WSOC from the urban (Granada) site influenced by a) a Saharan dust intrusion (23 July 2008) and b) a European air mass (17 September 2008; center), and c) after an experiment to collect diesel exhaust. Photos of each filter (a, b, and c) are shown in the middle panel. Air mass 5-day backward trajectories (bottom) from 500 m a.g.l. corresponding to 23 July 2008 at 0400 UTC (a) and 17 September 2008 at 0400 UTC (b) are shown in the bottom panel. UV–vis absorption curves for the three representative samples (Saharan-derived [gray], European-derived [black], and diesel experiment [dashed]) are shown at the bottom right.

3.3. PARAFAC results

From our dataset of EEM spectra, PARAFAC modeling resolved three fluorescent components (Fig. 3a). Each component is identified in Table S1 (Supplementary Data) along with a listing of similar components identified in other studies and their molecular association. C3 was similar in peak position to tryptophan, but overlapped more closely with naphthalene (Fig. 3b). C1, at ex/em of 240 (295)/402 nm (parentheses indicate shoulder or secondary excitation peak), was the most dominant component in all samples, ranging from 66% to 71% (Table 3). The relative amounts of C2, at ex/em of 255(365)/485 nm, and C3, at ex/em of 240(275)/332 nm, in Granada urban WSOC ranged from 13% to 19% and 12%–21%, respectively (Table 3). The %C3 was highest in samples from the diesel experiment (between 20% and 27%).

3.4. Aerosol columnar properties

Mean daily δ_{A440} ranged from 0.08 (Euro-derived) to 0.58 (Saharan-influenced). The ratio of $\delta_{A440}:\delta_{A1020}$ was greater for Euro-dominated days than for Saharan dust-dominated days (Table 4). Mean daily ω_{0A440} ranged from 0.83 to 0.93 and showed a spectral dependency, increasing with wavelength in Saharan-influenced

cases and decreasing or remaining constant in the Euro-dominated cases (Table 4). Mean daily g_{440} ranged from 0.67 to 0.75. For periods with Saharan aerosol intrusions, $\delta_{A\lambda}$ and g_{λ} were higher (Table 4). The α values were substantially higher for Euro-dominated days than for Saharan-influenced days (Table 4).

The radii of fine and coarse mode particles ranged from 0.140 μm (Euro) to 0.218 μm (Saharan) and from 1.8 μm (Saharan) to 5.0 μm (Euro), respectively, and the r_{eff} ranged from 0.47 to 1.29 μm (Table 5). V_f values (from 0.005 to 0.032 $\mu\text{m}^3 \mu\text{m}^{-2}$) were lower for Euro-dominated days, while V_c values (from 0.05 to 0.36 $\mu\text{m}^3 \mu\text{m}^{-2}$) were higher for Saharan-influenced days (Table 5).

3.5. Relationships between stable isotope, spectroscopic, and aerosol columnar properties

The $\delta^{13}\text{C}$ value was positively related to g_{440} and negatively related to α (Fig. 4). The $\delta^{15}\text{N}$ value was not significantly related to any columnar property.

The spectral slope ratio, S_R , was significantly and negatively related to WSOC air concentration and the effective radius of aerosol particles (Fig. 5). The HIX was significantly and positively related to g_{440} and r_f (Fig. 6a), with high HIX representing the Saharan-influenced aerosols. The %C3 was also significantly related

Table 1
Loadings and stable isotope signatures^a of PM₁₀ aerosol samples.

Sample	Source ^b /Treatment	TC loading ($\mu\text{g m}^{-3}$)	OC ^c loading ($\mu\text{g m}^{-3}$)	TN loading ($\mu\text{g m}^{-3}$)	OC ^c /TC (%)	TC/TN	$\delta^{13}\text{C}$ ‰ of TC (V-PDB)	$\delta^{13}\text{C}$ ‰ of OC (V-PDB)	$\delta^{15}\text{N}$ ‰ of TN (Air-N2)
Granada urban aerosols									
6-May	E	5.97	2.92	1.26	49	4.7	-22.89	-25.77	13.98
14-May	S	3.12	1.77	0.76	57	4.1	-24.40	-25.82	7.82
22-May	E	3.11	1.70	0.77	55	4.0	-24.38	-25.75	9.33
23-Jun	S	4.64	2.38	1.45	51	3.2	-21.10	-25.86	7.42
24-Jun ^d	E	10.6	2.08	1.03	20	10	-21.88	-25.83	11.59
4-Jul	E	4.72	2.26	1.08	48	4.4	-21.92	-25.86	10.53
12-Jul	E	3.46	1.79	0.68	52	5.1	-21.82	-26.46	11.84
23-Jul	S	4.82	2.44	1.27	51	3.8	-20.49	-25.85	8.26
30-Jul	S	4.88	1.88	1.10	39	4.4	-21.09	-27.05	9.93
6-Aug	S	3.00	2.01	0.86	67	3.5	-21.29	-25.87	8.77
13-Aug	S	3.83	1.48	0.82	39	4.7	-21.37	-26.52	7.86
20-Aug	E	4.73	2.34	0.83	50	5.7	-21.06	-26.48	9.56
26-Aug	E	3.55	1.84	1.24	52	2.9	-21.47	-26.48	8.01
10-Sep	E	5.28	2.72	0.64	51	8.3	-24.79	-26.41	6.08
17-Sep ^d	E	5.34	2.82	1.03	53	5.2	-23.36	-26.57	9.66
24-Sep	U	2.04	1.86	1.01	91	2.0	-24.90	-26.42	8.72
1-Oct	E	4.56	2.42	1.16	53	3.9	-24.36	-25.96	11.8
Sierra Nevada aerosols									
5-Aug	S	0.16	0.14	0.12	90	1.3	-20.16	-26.69	6.26
12-Aug	S	0.10	0.09	0.15	96	0.6	-21.18	-27.39	5.21
Diesel experiment aerosol									
22-Dec	Shaking	552	213	7.50	39	74	-26.40	-25.43	8.95

^a TC = total carbon; OC = total organic carbon; TN = total nitrogen; $\delta^{13}\text{C}$ = stable isotope of carbon; $\delta^{15}\text{N}$ = stable isotope of nitrogen.

^b S = Saharan-derived; E = Euro-derived; U = unknown or other.

^c OC may be biased toward higher values by elemental carbon (see Supporting Information, Detailed Methods).

^d High pollution.

to g_{440} and r_f (Fig. 6b). High %C3 corresponded to low g_{440} and r_f , characteristic of pollution aerosols.

4. Discussion

4.1. PM₁₀ aerosol and WSOC chemical properties

On a global scale, both dust transport and fossil fuel burning are on the rise (Prospero and Lamb, 2003; Liepert and Tegen, 2002). In densely populated urban and industrial areas, the organic aerosol content is higher than in remote sites due to fossil fuel and biofuel combustion (Bond et al., 2004). Indeed in our study, the TC, OC, and WSOC air concentrations were higher for urban Granada samples than remote Sierra Nevada samples.

The WSOC content we measured in urban aerosol samples (ranging from 1.67 to 2.38 $\mu\text{g m}^{-3}$) is at the low end of the range reported in other studies of urban aerosols (from 1.4 to 7.1 $\mu\text{g m}^{-3}$; Decesari et al., 2001; Ruellan and Cachier, 2001; Zappoli et al., 1999), but very similar to urban samples collected in the summer only (Decesari et al., 2001). In fact, in urban, agricultural, and

remote high mountain settings, summer WSOC values are almost always the lowest (Decesari et al., 2001; Ruellan and Cachier, 2001; Zappoli et al., 1999), which may be due to greater biomass burning (Jaffrezou et al., 2005) and shallow planetary boundary layer in the colder seasons, but also to the preferential shift of semi-volatile organic compounds from the particulate phase into the gas phase with increased summer temperatures (Anderson et al., 2008).

The influence of Saharan dust was seen in C and N stable isotopic signatures of PM₁₀ aerosols and WSOC optical properties. $\delta^{13}\text{C}$ and $\delta^{15}\text{N}$ clustered based on aerosol source, with more positive $\delta^{15}\text{N}$ and more negative $\delta^{13}\text{C}$ values representative of Euro-derived aerosols (Fig. 2). Samples with the Saharan dust influence generally had a more enriched $\delta^{13}\text{C}$ signature. The range of $\delta^{15}\text{N}$ values we observed for the Granada PM₁₀ samples is nearly identical to that observed in Paris PM₁₀ samples collected in the summer (Widory, 2007). The more enriched $\delta^{15}\text{N}$ signature and higher N content of the Granada urban aerosols compared to the remote Sierra Nevada samples is likely related to greater NO_x compounds present in aerosols from fossil fuel burning (Pichlmayer et al., 1998).

One of the most important results of this study is that the optical spectroscopic properties of WSOC and the isotopic values of PM₁₀ aerosols provide distinguishing signatures of urban pollution and Saharan dust aerosols. The stable isotopic, UV–vis absorbance, and fluorescence properties that we measured were consistent with what is known about the sources of PM₁₀ aerosols from their columnar properties. For instance, the diesel exhaust sample, one end member for the pollution influence in Granada, had the most negative $\delta^{13}\text{C}$ value, lowest S_R value, highest %C3, and lowest HIX. The significant relationships that emerged from this study suggest that days with more spherical particles (low g_λ value), characteristic of high pollution situations, will have more negative $\delta^{13}\text{C}$ values, higher %C3, and lower HIX values approaching those of diesel exhaust. In contrast, days with more asymmetric particles, characteristic of Saharan intrusion events (Lyamani et al., 2006a), had lower %C3 and higher HIX.

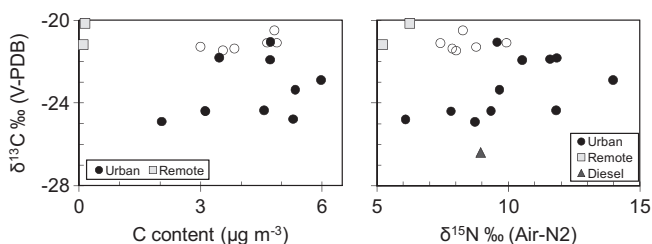


Fig. 2. Stable isotope and C air concentration data for PM₁₀ samples from the Granada urban area, a remote site in the Sierra Nevada mountains, Spain, and a diesel exhaust experiment. Empty circles indicate urban samples influenced by Saharan dust intrusions and filled circles indicate European (pollution) sources.

Table 2WSOC air concentration and UV–vis absorbance properties^a of WSOC extracted from PM₁₀ aerosol samples, diesel experiment samples, and control filter.

Date	Source ^b /treatment	WSOC($\mu\text{g m}^{-3}$)	$a_{250}(\text{m}^{-1} \text{ m}^{-3} \text{ L}^{-1})$	$a_{320}(\text{m}^{-1} \text{ m}^{-3} \text{ L}^{-1})$	$\epsilon_{250}(\text{m}^2 \text{ mmol}^{-1})$	$\epsilon_{320}(\text{m}^2 \text{ mmol}^{-1})$	$S_{275-295}(\text{nm}^{-1})$	S_R
Granada urban WSOC								
23-Jun	S	NSS	9.8E-03	4.3E-03	–	–	0.010	1.18
24-Jun	E	NSS	8.0E-03	3.6E-03	–	–	0.010	1.29
4-Jul	E	NSS	1.0E-02	5.5E-03	–	–	0.008	1.22
12-Jul	E	NSS	7.7E-03	3.9E-03	–	–	0.008	1.22
23-Jul	S	NSS	8.0E-03	3.8E-03	–	–	0.010	1.33
30-Jul	S	NSS	1.1E-02	5.5E-03	–	–	0.008	1.34
6-Aug	S	2.20 ± 0.013	9.1E-03	3.7E-03	49	20	0.011	1.30
13-Aug	S	NSS	7.8E-03	3.5E-03	–	–	0.010	1.40
20-Aug	E	2.38 ± 0.003	9.8E-03	4.1E-03	49	21	0.011	1.12
26-Aug	E	2.00 ± 0.004	9.1E-03	4.5E-03	55	27	0.009	1.36
10-Sep	E	2.03 ± 0.004	9.1E-03	4.0E-03	53	24	0.011	1.36
17-Sep ^d	E	1.74 ± 0.013	7.7E-03	3.5E-03	53	24	0.010	1.52
24-Sep	U	1.67 ± 0.002	6.4E-03	3.0E-03	46	22	0.011	1.47
1-Oct	E	2.11 ± 0.012	1.1E-02	5.0E-03	60	29	0.010	1.27
Sierra Nevada WSOC								
5-Aug	S	0.37 ± 0.029	3.5E-03	1.4E-03	56	22	0.014	1.83
12-Aug	S	0.25 ± 0.002	2.7E-03	1.1E-03	66	27	0.014	2.14
Diesel experiment WSOC								
22-Dec	Shaking	NSS	1.1E-02	3.1E-03	–	–	0.019	1.00
22-Dec	Shaking	NSS	1.1E-02	2.9E-03	–	–	0.019	0.95
22-Dec	Sonication	NSS	1.1E-02	2.8E-03	–	–	0.019	0.92
22-Dec	Sonication	NSS	1.0E-02	2.6E-03	–	–	0.019	0.95
Control filter WSOC ^c								
12-Dec	NA	(0.09)	NA	(0.16)	0	1.8	NA	NA

^a WSOC = water soluble organic carbon; a_{250} = absorption at 250 nm; a_{320} = absorption at 320 nm; ϵ_{250} = molar absorption at 250 nm; ϵ_{320} = molar absorption at 320 nm; $S_{275-295}$ = spectral slope between 275 and 295 nm; S_R = spectral slope ratio. Absorption (m^{-1}) normalized to volume air sampled (m^3) and volume of extractant used (L). NSS = not sufficient sample. NA = not applicable. Dash indicates that value could not be calculated due to insufficient sample for DOC concentration measurements.

^b S = Saharan-derived; E = Euro-derived; U = unknown or other. Results of duplicate diesel experiment samples extracted by mechanical shaking and sonication are shown.

^c Values for $\frac{1}{4}$ of filter extracted in 75 mL of milli-Q water have units of mg L^{-1} for WSOC concentration, m^{-1} for absorption, and $\text{m}^2 \text{ mmol}^{-1}$ for molar absorption. Parentheses indicate different units were used.

^d High pollution.

These relationships are consistent with the sources of these organic aerosols and the environmental transformations expected to affect them. For example, component 3 has a similar fluorescence peak to naphthalene, a compound in diesel exhaust. The greater contribution of C3 to the total fluorescence of the diesel exhaust

sample as well as the significant inverse relationship between %C3 and g_λ value (with low g_λ representative of pollution situations) suggests that the diesel influence may be traced by this component. In terms of aerosol transformation, aerosols traveling from the Sahara (highest HIX) are in the atmosphere for a longer period than

Table 3Fluorescence properties^a of WSOC extracted from PM₁₀ aerosol samples, diesel experiment samples, and control filter.

Date	Source ^b /Treatment	FI	HIX	F_{total} (RU)	%C1	%C2	%C3	f_{total} (RU L mg^{-1})	f_{C1} (RU L mg^{-1})	f_{C2} (RU L mg^{-1})	f_{C3} (RU L mg^{-1})
Granada urban WSOC											
23-Jun	S	1.48	3.61	3.78	70%	14%	16%	–	–	–	–
24-Jun	E	1.56	3.50	3.55	71%	13%	17%	–	–	–	–
4-Jul	E	1.56	3.41	4.14	68%	16%	16%	–	–	–	–
12-Jul	E	1.52	4.64	2.42	67%	19%	14%	–	–	–	–
23-Jul	S	1.52	4.89	2.47	71%	17%	12%	–	–	–	–
30-Jul	S	1.49	4.30	4.16	70%	16%	14%	–	–	–	–
6-Aug	S	1.59 ^c	4.11	3.19	71%	15%	14%	0.74	0.15	0.15	1.04
13-Aug	S	1.53	4.69	2.81	69%	17%	14%	–	–	–	–
20-Aug	E	1.50	3.19	4.22	67%	14%	18%	0.86	0.18	0.23	1.27
26-Aug	E	1.64	P	P	P	P	P	P	P	P	P
10-Sep	E	1.59	3.14	4.94	67%	14%	19%	1.18	0.25	0.34	1.76
17-Sep ^d	E	1.61	2.79	3.60	66%	14%	21%	1.00	0.21	0.32	1.52
24-Sep	U	1.52	4	2.09	69%	17%	14%	0.64	0.16	0.13	0.93
1-Oct	E	1.52	3.54	5.22	71%	14%	16%	1.27	0.24	0.28	1.79
Diesel experiment WSOC											
22-Dec	Shaking	1.54	2.84	0.28	74%	7%	20%	–	–	–	–
22-Dec	Shaking	1.56	2.77	0.25	74%	6%	19%	–	–	–	–
22-Dec	Sonication	1.58	1.91	0.23	68%	5%	26%	–	–	–	–
22-Dec	Sonication	1.56	1.97	0.24	69%	5%	26%	–	–	–	–

^a FI = fluorescence index; HIX = humification index; F_{total} = total fluorescence loading; C1 = PARAFAC component 1; C2 = PARAFAC component 2; C3 = PARAFAC component 3; P = inadequate PARAFAC fit; Dash indicates that value could not be calculated due to insufficient sample for DOC concentration measurements.

^b S = Saharan-derived; E = Euro-derived; U = unknown or other.

^c The FI was calculated as the ratio of emission intensities at 480:530 nm because FI peak position was shifted from its expected position (450 nm) to between 460 and 465 nm.

^d High pollution.

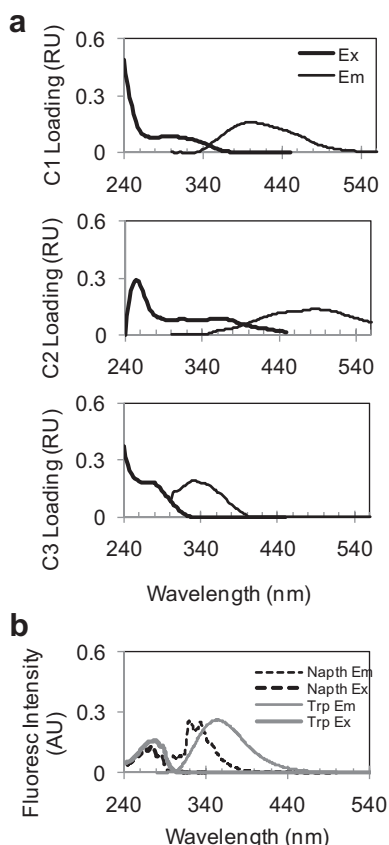


Fig. 3. (a) The spectral loading (RU) of three components validated by the PARAFAC model and (b) the fluorescence intensities (arbitrary units (AU)) of Naphthalene (Naph) dissolved in cyclohexane and Tryptophan (Trp) dissolved in water (source: Du et al., 1998).

the Euro-derived aerosols (intermediate HIX) or diesel exhaust (lowest HIX) and are expected to undergo intense photoreactions and chemical transformations (eg. Aymoz et al., 2004; Rudich et al., 2007), which result in aging of the organic aerosol and potentially higher C:H ratios (Heald et al., 2010). A higher HIX value, which reflects a shift of the fluorescence spectra toward longer emission wavelengths, is indicative of more condensed molecules and an increase in C:H ratios (Zsolnay, 2003). Although the HIX has been applied primarily in the study of soil and aquatic organic matter, the underlying chemical changes (increase in the C:H ratio) are consistent with aging of aerosols.

Significant negative relationships between S_R and WSOC air concentration and r_{eff} (Fig. 5) may provide further insights into the size of Euro-derived aerosol particles compared to Saharan-influenced aerosols. In aquatic environments, shifts in the S_R reflect changes in the ratio of low molecular weight (LMW):high molecular weight (HMW) compounds and changes due to photobleaching of dissolved organic matter (Helms et al., 2008). The combination of low S_R and higher effective radius (Fig. 5), which is generally more the case for urban aerosols than Saharan dust aerosols, may suggest that the optically-active WSOC in urban air masses comprise more HMW compounds or have received less light-exposure than the Saharan-influenced samples.

As the major contributor to urban aerosol fluorescence, representing >70% of the total fluorescence in all urban samples, the provenance of humic-like components C1 and C2 is also important. In studies conducted in redox-sensitive environments, a quinone-like component was identified that is similar to C1 (Fellman et al., 2009; Cory and McKnight, 2005). Component 2 (C2) has been identified as a terrestrial humic or fulvic acid-like component (Table 3). Quinones are major contributors to humic and fulvic acids with observed fluorescence at higher emission wavelengths (Cory and McKnight, 2005). Some quinones, such as hydroxyquinone, are known reactive oxygen species and are associated with asthma and respiratory illness (Cho et al., 2004) and quinones are formed by PAH photodegradation (Vione et al., 2006). The potential

Table 4
Columnar properties^a (daily mean value with standard deviation) for select dates in summer 2008 at Granada, Spain.

Date	Source ^b	$\delta_{A\lambda}$				$\delta_{A440:1020}$	$\omega_{0A\lambda}$				g_{λ}				α
		1020	870	670	440		1020	870	670	440	1020	870	670	440	
23-Jun	S	0.45 ±0.07	0.48 ±0.07	0.51 ±0.06	0.58 ±0.04	1.28	0.94 ±0.03	0.94 ±0.03	0.93 ±0.03	0.91 ±0.04	0.70 ±0.04	0.71 ±0.04	0.72 ±0.04	0.73 ±0.02	0.28 ±0.06
24-Jun	E	0.05 ±0.01	0.06 ±0.01	0.07 ±0.01	0.11 ±0.03	2.22	0.86 ±0.04	0.86 ±0.04	0.87 ±0.03	0.89 ±0.02	0.65 ±0.02	0.64 ±0.02	0.65 ±0.02	0.70 ±0.01	0.93 ±0.16
4-Jul	E	0.09 ±0.04	0.10 ±0.05	0.10 ±0.05	0.13 ±0.06	1.46	0.85 ±0.04	0.84 ±0.04	0.83 ±0.04	0.83 ±0.03	0.70 ±0.03	0.69 ±0.02	0.70 ±0.02	0.72 ±0.02	0.58 ±0.19
12-Jul	E	0.04 ±0.001	0.05 ±0.01	0.05 ±0.003	0.08 ±0.01	1.77	0.85 ±0.02	0.85 ±0.02	0.85 ±0.01	0.87 ±0.01	0.67 ±0.01	0.66 ±0.01	0.68 ±0.01	0.72 ±0.01	0.81 ±0.16
23-Jul	S	0.25 ±0.05	0.28 ±0.05	0.28 ±0.05	0.31 ±0.06	1.21	0.92 ±0.05	0.91 ±0.05	0.90 ±0.05	0.87 ±0.06	0.72 ±0.04	0.72 ±0.04	0.73 ±0.04	0.75 ±0.03	0.25 ±0.32
30-Jul	S	0.20 ±0.04	0.22 ±0.05	0.23 ±0.04	0.27 ±0.05	1.31	0.92 ±0.02	0.91 ±0.02	0.89 ±0.03	0.88 ±0.03	0.70 ±0.03	0.70 ±0.03	0.71 ±0.03	0.73 ±0.02	0.35 ±0.61
6-Aug	S	0.15 ±0.04	0.17 ±0.03	0.16 ±0.04	0.20 ±0.05	1.34	0.89 ±0.03	0.88 ±0.03	0.86 ±0.03	0.85 ±0.03	0.70 ±0.02	0.70 ±0.02	0.71 ±0.02	0.73 ±0.02	0.36 ±0.05
13-Aug	S	0.18 ±0.04	0.19 ±0.05	0.20 ±0.05	0.24 ±0.06	1.33	0.92 ±0.03	0.91 ±0.03	0.89 ±0.03	0.88 ±0.03	0.69 ±0.02	0.69 ±0.02	0.70 ±0.02	0.72 ±0.01	0.38 ±0.07
20-Aug	E	0.05 ±0.02	0.06 ±0.02	0.06 ±0.02	0.10 ±0.03	2.00	0.83 ±0.02	0.83 ±0.02	0.84 ±0.02	0.87 ±0.02	0.68 ±0.02	0.67 ±0.02	0.67 ±0.02	0.70 ±0.02	0.93 ±0.19
26-Aug	E	0.09 ±0.02	0.10 ±0.02	0.11 ±0.02	0.19 ±0.04	2.19	0.88 ±0.05	0.87 ±0.05	0.88 ±0.04	0.90 ±0.03	0.65 ±0.03	0.64 ±0.03	0.64 ±0.03	0.67 ±0.01	1.05 ±0.010
17-Sep ^c	E	0.11	0.13	0.15	0.25	2.26	0.92	0.91	0.92	0.93	0.65	0.65	0.66	0.69	0.85
1-Oct	E	0.07	0.09	0.12	0.24	3.38	0.88	0.89	0.91	0.93	0.58	0.59	0.63	0.70	1.19

^a $\delta_{A\lambda}$ = aerosol optical depth (dimensionless) at 440, 670, 870 and 1020 nm; $\omega_{0A\lambda}$ = single scattering albedo (dimensionless); g_{λ} = asymmetry parameter (dimensionless); α = Angström wavelength exponent (dimensionless). Dash indicates no data were recorded on that day.

^b S = Saharan-derived; E = Euro-derived; U = unknown or other.

^c High pollution.

Table 5
Columnar properties^a (daily mean value with standard deviation) for select dates in summer 2008 at Granada, Spain.

Date	Source ^b	r _f (μm)	r _c (μm)	r _{eff} (μm)	V _f (μm ³ μm ⁻²)	V _c (μm ³ μm ⁻²)	V _f :V _c
23-Jun	S	0.214 ±0.078	1.91 ±0.37	0.93 ±0.23	0.032 ±0.011	0.36 ±0.09	0.09 ±0.030
24-Jun	E	0.168 ±0.012	3.73 ±1.66	0.93 ±0.50	0.008 ±0.002	0.05 ±0.02	0.18 ±0.10
4-Jul	E	0.166 ±0.016	3.58 ±1.79	1.29 ±0.69	0.008 ±0.004	0.09 ±0.01	0.09 ±0.05
12-Jul	E	0.184 ±0.010	4.21 ±0.59	1.23 ±0.23	0.005 ±0.0003	0.05 ±0.01	0.10 ±0.02
23-Jul	S	0.218 ±0.027	1.88 ±0.30	0.93 ±0.14	0.017 ±0.004	0.18 ±0.05	0.09 ±0.02
30-Jul	S	0.174 ±0.016	1.92 ±0.43	0.84 ±0.10	0.015 ±0.004	0.16 ±0.05	0.10 ±0.02
6-Aug	S	0.206 ±0.024	2.67 ±0.83	1.10 ±0.30	0.010 ±0.003	0.12 ±0.04	0.09 ±0.03
13-Aug	S	0.185 ±0.015	1.82 ±0.32	0.85 ±0.10	0.013 ±0.003	0.13 ±0.04	0.10 ±0.02
20-Aug	E	0.149 ±0.012	4.96 ±0.40	1.24 ±0.20	0.007 ±0.002	0.08 ±0.04	0.09 ±0.03
26-Aug	E	0.140 ±0.011	3.86 ±1.24	0.75 ±0.26	0.015 ±0.003	0.10 ±0.05	0.18 ±0.09
17-Sep ^c	E	0.154	3.09	0.54	0.022	0.09	0.25
1-Oct	E	0.176	4.06	0.47	0.022	0.05	0.46

^a r_f = radius of fine mode particles; r_c = radius of coarse mode particles; r_{eff} = effective radius; V_f = volume concentration of fine mode particles; V_c = volume concentration of coarse mode particles; V_f:V_c = ratio of volume concentration of fine to coarse mode particles. Dash indicates no data were recorded on that day.

^b S = Saharan-derived; E = Euro-derived; U = unknown or other.

^c High pollution days.

contribution of quinone compounds to aerosol fluorescence, therefore, is an important area of future research with implications for human respiratory health.

4.2. Methodological considerations for organic aerosol characterization

Our results identified important methodological considerations regarding sampling, sample extraction, and fluorescence interpretation. First, the results from our control filter indicated that exposure to ambient air did not result in additional adsorption of fluorescent organic substances (Supplementary Data, Section 2). The main bias in this study is with respect to the OC air concentrations for the urban samples, which may be biased toward higher values due to potential incomplete removal of EC during sample preparation (Supplementary Materials).

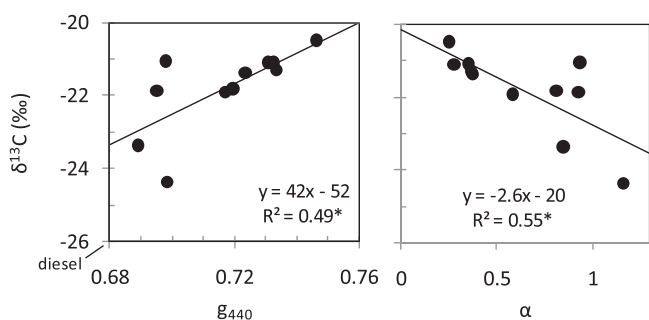


Fig. 4. Relationships between the stable C isotope signature and asymmetry parameter at 440 nm (g₄₄₀) and Angstrom exponent (α) recorded on the same dates. Only significant relationships are shown. *p < 0.05.

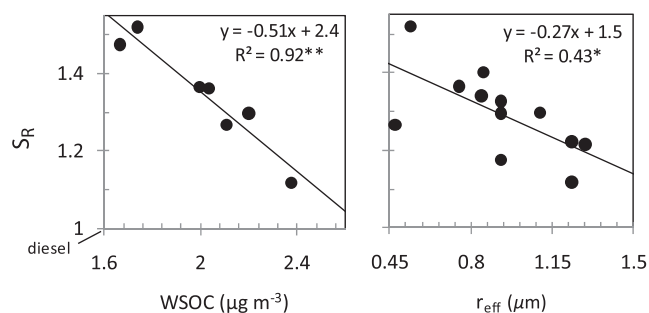


Fig. 5. Relationships between the spectral slope ratio (S_R) and WSOC air concentration and effective radius (r_{eff}) measured on the same dates. Only significant relationships are shown. **p < 0.01; *p < 0.05.

In terms of WSOC extraction, shaking and sonication extraction methods did influence fluorescence properties. The HIX was substantially lower and the amount of C3 increased when sonication was used compared to shaking. The total fluorescence loading (F_{total}) was nearly the same in shaking and sonication extractions (Table 3), suggesting that the same amount of fluorescent material was liberated by both methods. In other words, sonication probably did not mobilize additional material, but may have instead transformed the organic material. We would not expect mechanical shaking to alter the chemical composition of dissolved organic matter, but sonication has been shown to induce destruction of intact macromolecules (Stemmer et al., 1998), and this larger particle breakdown would be consistent with the lower HIX (fewer condensed molecules) observed in sonicated samples. These differences between mechanical shaking and sonication are important considerations for studies using fluorescence to characterize WSOC.

In our study, PARAFAC modeling identified three components previously reported in the literature (Supplementary Data, Table S1). It has been recognized that these components represent the dominant fluorescing moieties in dissolved organic matter and that

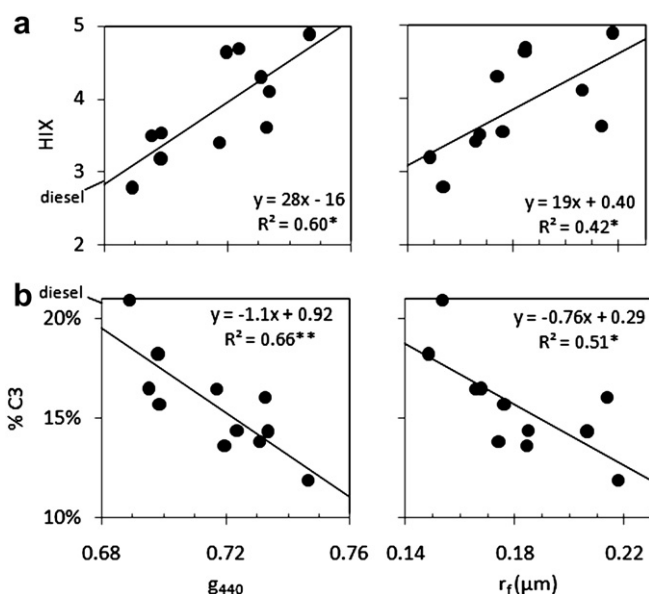


Fig. 6. Relationships between WSOC fluorescence properties, a) humification index and asymmetry parameter (g₄₄₀), radius of fine mode particles (r_f), and b) Component 3 (%C3) and g₄₄₀ and r_f. Only significant relationships are shown. **p < 0.01; *p < 0.05.

additional components would be resolved in a larger dataset (Holbrook et al., 2006). Component 3 (C3) has a fluorescence spectrum (peak ex/em of 275/332 nm; Fig. 3a) very similar to diesel fuel (ex/em of 270/334 nm) (Courvoisier et al., 2006) and extracts of naphthalene (ex/em of 275/334 nm) and tryptophan (ex/em of 275/340 nm) (Du et al., 1998). In the diesel experiment, C3 is related to the organic compounds released from diesel combustion and not to aromatic amino acids. This demonstrates that caution must be taken when interpreting the nature of compounds from fluorescence peaks. For example, in the study of Nakajima et al. (2008), a fluorescent peak at a similar location, at ex/em of 260–290/305–345 nm and present only in winter aerosol samples, was attributed to fluorescence from tyrosine and tryptophan, but our study suggests that a winter-time fossil fuel burning fluorescence signal may also be considered.

In situ fluorescence monitoring (Pinnick et al., 2004; Pan et al., 2009) has great potential for source apportionment of organic aerosols, and its use for measurements of biological aerosols has already been established at remote sites. The amount of C3 may be a useful metric for monitoring diesel pollution. However, given the similarities between the fluorescence spectra of diesel exhaust and tryptophan, associated with biological aerosols (Pan et al., 2009), multiple fluorescence wavelengths may need to be monitored to distinguish sources. Also, time resolved fluorescence can provide a fourth dimension for organic matter source discrimination.

5. Conclusions

To our knowledge, this is the first study to relate columnar properties of urban aerosols with WSOC spectroscopic properties and the first to quantitatively characterize three-dimensional fluorescent components of urban aerosol WSOC with PARAFAC. We found several significant relationships between WSOC spectroscopic properties and columnar properties related to size (r_f) and shape (g_λ), which suggest that the water soluble organic fraction has some bearing on the physical properties of the total aerosol. We also found that UV–vis and fluorescence spectroscopy and stable isotope signatures of C and N were able to differentiate organic aerosols from Saharan origin and urban air pollution in an urban setting. In particular, the following key findings provide important information for the characterization of organic aerosols in urban environments:

- 1) Greater fluorescence in the region of C3 reflected increased diesel pollution and this component could potentially be used to track the urban pollution signal,
- 2) The humification index may be an indication of aerosol aging, particularly in Saharan-influenced urban air,
- 3) Low S_R values may reflect higher molecular weight compounds in Euro-derived than Saharan-influenced aerosols

The use of UV–vis absorbance and fluorescence spectroscopy for WSOC characterization is on the rise. Our study suggests that the use of these fairly low-cost, rapid techniques to discriminate organic aerosol sources is especially valuable for urban centers that are subject to substantial diesel and other fossil fuel pollution or receive dust deposition, such as those in the Mediterranean region, where Saharan dust intrusion events are frequent and widespread. Columnar aerosol properties already distinguish the physical characteristics of major aerosol sources, based on aerosol scattering and absorption. These data are available at very frequent time steps (minutes or hours). Fluorescence spectroscopy, on the other hand, takes longer (although much less time than GC–MS analyses, for example) and, at least at present, requires a water extraction, but offers more detailed information about the light absorbing organic

matter in aerosols. This study has shown that fluorescence spectroscopy supports columnar information from sun photometry and provides chemical information that is consistent with organic aerosol sources and transformations. These findings are extremely important in regards to 1) potentially augmenting the vast dataset of global columnar measurements, 2) developing new instruments for in situ monitoring of organic aerosols, and 3) improving our understanding of the chemical character and optical properties of organic aerosols.

Acknowledgments

We would like to thank R. D. McGrath for DOC concentration analyses and S. Kim for editing assistance. The authors gratefully acknowledge the National Oceanic and Atmospheric Administration (NOAA) Air Resources Laboratory (ARL) for use of the HYbrid Single-Particle Lagrangian Integrated Trajectory (HYSPPLIT) model and Real-time Environmental Applications and Display sYstem (READY) website and the National Aeronautics and Space Administration (NASA) OMI for ozone measurements. Funding was provided by BBVA through the ECOSENSOR project, the Andalusian Regional Government through project P08-RNM-3568, the Spanish Ministry of Science and Technology through project CGL2010-18782, and the Spanish Ministry of the Environment through the MICROBIOGEOGRAPHY (080/2007) project, and the University of Colorado provided support through the Undergraduate Research Opportunities Program.

Appendix. Supplementary material

Supplementary material associated with this paper can be found, in the online version, at doi:10.1016/j.atmosenv.2011.01.029.

References

- Alados-Arboledas, L., Lyamani, H., Olmo, F.J., 2003. Aerosol size properties at Armilla, Granada (Spain). *Q. J. Roy. Meteor. Soc.* 129 (590), 1395–1413.
- Anderson, C., Dibb, J.E., Griffin, R.J., Bergin, M.H., 2008. Simultaneous measurements of particulate and gas-phase water-soluble organic carbon concentrations at remote and urban-influenced locations. *Geophys. Res. Lett.* 35, L13706. doi:10.1029/2008GL033966.
- Andreae, M.O., Gelencser, A., 2006. Black carbon or brown carbon? The nature of light-absorbing carbonaceous aerosols. *Atmos. Chem. Phys.* 6, 3131–3148.
- Aymoz, G., Jaffrezou, J.L., Jacob, V., Colomb, A., George, C., 2004. Evolution of organic and inorganic components of aerosol during a Saharan dust episode observed in the French Alps. *Atmos. Chem. Phys.* 4, 2499–2512.
- Baeza-Squiban, A., Boland, S., Fournier, T., 1999. Diesel exhaust particles are taken up by human airway epithelial cells in vitro and alter cytokine expression. *Am. J. Phys.* 276, L604–L613.
- Bond, T.C., Klimont, Z., Nelson, S.M., Streets, D.G., Woo, J., Yarber, K.F., 2004. A technology-based global inventory of black and organic carbon emissions from combustion. *J. Geophys. Res.* 109, D14203. doi:10.1029/2003JD003697.
- Cachier, H., 1989. Isotopic characterization of carbonaceous aerosols. *Aerosol. Sci. Technol.* 10, 379–385.
- Cho, A.K., Stefano, E.D., You, Y., Rodriguez, C.E., Schmitz, D.A., Kumagai, Y., Miguel, A.H., Eiguren-Fernandez, A., Kobayashi, T., Avol, E., Froines, J.R., 2004. Determination of four quinones in diesel exhaust particles, SRM 1649a, and atmospheric PM_{2.5}. *Aerosol. Sci. Technol.* 38 (S1), 68–81.
- Cory, R.M., McKnight, D.M., 2005. Fluorescence spectroscopy reveals ubiquitous presence of oxidized and reduced quinones in dissolved organic matter. *Environ. Sci. Technol.* 39, 8142–8149.
- Courvoisier, F., Boutou, V., Guyon, L., Roth, M., Rabitz, H., Wolf, J., 2006. Discriminating bacteria from other atmospheric particles using femtosecond molecular dynamics. *J. Photochem. Photobiol. A: Chem.* 180, 300–306.
- Decesari, S., Facchini, M.C., Matta, E., Lettin, F., Mircea, M., Fuzzi, S., Tagliavini, E., Putaud, J.P., 2001. Chemical features and seasonal variation of fine aerosol water-soluble organic compounds in the Po Valley, Italy. *Atmos. Environ.* 35, 3691–3699.
- Draxler, R.R., Rolph, G.D., 2003. HYSPPLIT (HYbrid Single-Particle Lagrangian Integrated Trajectory) Model Access via NOAA ARL READY Website (<http://www.arl.noaa.gov/ready/hysplit4.html>).

- Du, H., Fuh, R.A., Li, J., Corkan, A., Lindsey, J.S., 1998. PhotochemCAD: a computer-aided design and research tool in photochemistry. *Photochemistry and Photobiology* 68, 141–142.
- Duarte, R.M.B.O., Pio, C.A., Duarte, A.C., 2004. Synchronous scan and excitation-emission matrix fluorescence spectroscopy of water-soluble organic compounds in atmospheric aerosols. *J. Atmos. Chem.* 48, 157–171.
- Duarte, R.M.B.O., Pio, C.A., Duarte, A.C., 2005. Spectroscopic study of the water-soluble organic matter isolated from atmospheric aerosols collected under different atmospheric conditions. *Anal. Chim. Acta.* 530, 7–14.
- Fellman, J.B., Miller, M.P., Cory, R.M., D'Amore, D.V., White, D., 2009. Characterizing dissolved organic matter using PARAFAC modeling of fluorescence spectroscopy: a comparison of two Models. *Environ. Sci. Technol.* 43, 6228–6234.
- Heald, C.L., Kroll, J.L., Jimenez, J.L., Docherty, K.S., DeCarlo, P.F., Aiken, A.C., Chen, Q., Martin, S.T., Farmer, D.K., Artaxo, P., 2010. A simplified description of the evolution of organic aerosol composition in the atmosphere. *Geophys. Res. Lett.* 37, L08803. doi:10.1029/2010GL042737.
- Helms, J.R., Stubbins, A., Ritchie, J.D., Minor, E.C., Kieber, D.J., Mopper, K., 2008. Absorption spectral slopes and slope ratios as indicators of molecular weight, source, and photobleaching of chromophoric dissolved organic matter. *Limnol. Oceanogr.* 53 (3), 955–969.
- Holben, B.N., Eck, T.F., Slutsker, I., Tanre, D., Buis, J.P., Setzer, A., Vermote, E., Reagan, J.A., Kaufman, Y.J., Nakajima, T., Lavenu, F., Jankowiak, I., Smirnov, A., 1998. Aeronet- a federated instrument network and data archive for aerosol characterization. *Remote Sensing Environ.* 66, 1–19.
- Holbrook, D.R., Yen, J.H., Grizzard, T.J., 2006. Characterizing natural organic material from the Occoquan Watershed (Northern Virginia, US) using fluorescence spectroscopy and PARAFAC. *Sci. Total. Environ.* 361, 249–266.
- Jacobson, M.C., Hansson, H.C., Noone, K.J., Charlson, R.J., 2000. Organic atmospheric aerosols: review and state of the science. *Rev. Geophys.* 38, 267–294.
- Jaffrezo, J.L., Aymoz, G., Delaval, C., Cozic, J., 2005. Seasonal variations of the water soluble organic carbon mass fraction of aerosol in two valleys of the French Alps. *Atmos. Chem. Phys.* 5, 2809–2821.
- Kieber, R.J., Whitehead, R.F., Reid, S.N., Willey, J.D., Seaton, P.J., 2006. Chromophoric dissolved organic matter (CDOM) in rainwater, southeastern North Carolina, USA. *J. Atmos. Chem.* 54, 21–41.
- Kneizys, F.X., Shettle, E.P., Abreu, L.W., Chetwind, J.H., Anderson, G.P., Gallery, W.O., Selby, J.E.A., Clough, S.A., 1988. Users Guide to LOWTRAN7. Environment Research Paper 1010. US Air Force Geophysics Laboratory, Bedford, MA.
- Liepert, B., Tegen, I., 2002. Multi-Decadal solar radiation trends in the United States and Germany and direct tropospheric aerosol forcing 107, D12. doi:10.1029/2001JD000760.
- Lyamani, H., Olmo, F.J., Alados-Arboledas, L., 2005. Saharan dust outbreak over south-eastern Spain as detected by sun photometer. *Atmos. Environ.* 39, 7276–7284.
- Lyamani, H., Olmo, F.J., Alcántara, A., Alados-Arboledas, L., 2006a. Atmospheric aerosols during the 2003 heat wave in southeastern Spain II: microphysical columnar properties and radiative forcing. *Atmos. Environ.* 40, 6465–6476.
- Lyamani, H., Olmo, F.J., Alcántara, A., Alados-Arboledas, L., 2006b. Atmospheric aerosols during the 2003 heat wave in southeastern Spain I: spectral optical depth. *Atmos. Environ.* 40, 6453–6464.
- Maria, S.F., Russell, L.M., Gilles, M.K., Myrnes, S.C.B., 2004. Organic aerosol growth mechanisms and their climate-forcing implications. *Science* 306, 1921–1924. doi:10.1126/science.1103491.
- Mladenov, N., Pulido-Villena, E., Morales-Baquero, R., Ortega-Retuerta, E., Sommaruga, R., Reche, I., 2008. Spatio-temporal drivers of dissolved organic matter in high alpine lakes: the role of Saharan dust inputs and bacterial activity. *J. Geophys. Res.* 113, G00D01. doi:10.1029/2008JG000699.
- Mladenov, N., López-Ramos, J., McKnight, D.M., Reche, I., 2009. Alpine lake optical properties as sentinels of dust deposition and global change. *Limnol. Oceanogr.* 54, 2386–2400.
- Mladenov, N., Reche, I., Olmo-Reyes, F.J., Lyamani, H., Alados-Arboledas, L., 2010. Relationships between spectroscopic properties of high-altitude organic aerosols and Sun photometry from ground-based remote sensing. *J. Geophys. Res.* 115. doi:10.1029/2009JG000991.
- Morales-Baquero, R., Pulido-Villena, E., Reche, I., 2006. Atmospheric inputs of phosphorus and nitrogen to the southwest Mediterranean region: biogeochemical responses of high mountain lakes. *Limnol. Oceanogr.* 51 (2), 830–837.
- Morris, D.P., Zagarese, H., Williamson, C.E., Balseiro, E.G., Hargreaves, B.R., Modenutti, B., Moeller, R., Queimalinos, C., 1995. The attenuation of solar UV radiation in lakes and the role of dissolved organic carbon. *Limnol. Oceanogr.* 40, 1381–1391.
- Muller, C.L., Baker, A., Hutchinson, R., Fairchild, I.J., Chris Kidd, C., 2008. Analysis of rainwater dissolved organic carbon compounds using fluorescence spectro-photometry. *Atmos. Environ.* 42, 8036–8045.
- Nakajima, H., Okada, K., Kuroki, Y., Nakama, Y., Handa, D., Arakaki, T., Tanahara, A., 2008. Photochemical formation of peroxides and fluorescence characteristics of the water-soluble fraction of bulk aerosols collected in Okinawa, Japan. *Atmos. Environ.* 42, 3046–3058.
- Nakajima, T., Tonna, G., Rao, R., Boi, P., Kaufmann, Y.J., Holben, B.N., 1996. Use of the brightness measurements from ground for remote sensing of particulate polydispersions. *Appl. Opt.* 35, 2672–2686.
- Olmo, F.J., Quirantes, A., Alcántara, A., Lyamani, H., Alados-Arboledas, L., 2006. Preliminary results of a non-spherical aerosol method for the retrieval of the atmospheric aerosol optical properties. *J. Quant. Spectrosc. Radiat. Transf.* 100, 305–314.
- Olmo, F.J., Quirantes, A., Lara, V., Lyamani, H., Alados-Arboledas, L., 2008. Aerosol optical properties assessed by an inversion method using the solar principal plane for non-spherical particles. *J. Quant. Spectrosc. Radiat. Transf.* 109, 1504–1516.
- Pan, Y., Pinnick, R.G., Hill, S.C., Chang, R.K., 2009. Particle-fluorescence spectrometer for real-time single-particle measurements of atmospheric organic carbon and biological aerosol. *Environ. Sci. Technol.* 43 (2), 429–434. doi:10.1021/es801544y.
- Perez, L., Tobias, A., Querol, X., Kunzli, N., Pey, J., Alastuey, A., Viana, M., Valero, N., Gonzalez-Cabree, M., Sunyer, J., 2008. Coarse particles from saharan dust and daily mortality. *Epidemiology* 19 (6), 800–807.
- Perrino, C., Canepari, S., Catrambone, M., Torre, S.D., Rantica, E., Sargolini, T., 2009. Influence of natural events on the concentration and composition of atmospheric particulate matter. *Atmos. Environ.* 43 (31), 4766–4779.
- Pichlmayer, F., Schoner, W., Seibert, P., Stihler, W., Wagenbach, D., 1998. Stable isotope analysis for characterization of pollutants at high elevation alpine sites. *Atmos. Environ.* 32 (23), 4075–4085.
- Pinnick, R.G., Hill, S.C., Pan, Y., Chang, R.K., 2004. Fluorescence spectra of atmospheric aerosol at Adelphi, Maryland, USA: measurement and classification of single particles containing organic carbon. *Atmos. Environ.* 38, 1657–1672.
- Prospero, J.M., Lamb, P.J., 2003. African droughts and dust transport to the Caribbean: climate change implications. *Science* 302, 1024–1027. doi:10.1126/science.1089915.
- Rudich, Y., Donahue, N.M., Mentel, T.F., 2007. Aging of organic aerosol: bridging the gap between laboratory and field studies. *Annu. Rev. Phys. Chem.* 58, 321–352.
- Ruellan, S., Cachier, H., 2001. Characterisation of fresh particulate vehicular exhausts near a Paris high flow road. *Atmos. Environ.* 35, 453–468.
- Schefub, E., Rattmeyer, V., Stuetz, J.W., Jansen, J.H.F., Sminninghe Damst, J.S., 2003. Carbon isotope analyses of n-alkanes in dust from the lower atmosphere over the central eastern Atlantic. *Geochimica et Cosmochimica Acta* 60 (10), 1757–1767.
- Schütz, L., Jaenicke, R., Pietrek, H., 1981. Saharan dust transport over the North Atlantic Ocean, desert dust: origin, characteristics, and effects on man. *Geol. Soc. America* 186, 87–100.
- Stedmon, C.A., Markager, S., Bro, R., 2003. Tracing dissolved organic matter in aquatic environments using a new approach to fluorescence spectroscopy. *Mar. Chem.* 82, 239–254.
- Stedmon, C.A., Bro, R., 2008. Characterizing dissolved organic matter fluorescence with parallel factor analysis: a tutorial. *Limnol. Oceanogr. Methods* 6, 572–579.
- Stemmer, M., Gerzabek, M.H., Kandeler, E., 1998. Organic matter and enzyme activity in particle-size fractions of soils obtained after low-energy sonication. *Soil. Biol. Biochem.* 30 (1), 9–17.
- Smirnov, A., Holben, B.N., Eck, T.F., Dubovik, O., Slutsker, I., 2000. Cloud-screening and quality control algorithms for the AERONET database. *Remote Sensing Environ.* 73 (3), 337–349.
- Sun, H., Biedermann, L., Bond, T.C., 2007. The color of brown carbon: a model for ultraviolet and visible light absorption by organic carbon aerosol. *Geophys. Res. Lett.* 34, L17813. doi:10.1029/2007GL029797.
- Viana, M., Chi, X., Maenhaut, W., Cafmeyer, J., Querol, X., Alastuey, A., Mikuska, P., Vecera, Z., 2006. Influence of sampling artefacts on measured PM₁₀, OC, and EC levels in carbonaceous aerosols in an urban area. *Aerosol. Sci. Technol.* 40, 107–117.
- Vione, D., Maurino, V., Minero, C., Pelizzetti, E., Harrison, M.A.J., Olariu, R., Arsene, C., 2006. Photochemical reactions in the tropospheric aqueous phase and on particulate matter. *Chem. Soc. Rev.* 35, 441–453. doi:10.1039/b510796m.
- Washington, R., Todd, M., Middleton, N.J., Goudie, A.S., 2003. Dust-storm source areas determined by the total ozone monitoring spectrometer and surface observations. *Ann. Assoc. Am. Geogr.* 93 (2), 297–313.
- Weishaar, J.L., Aiken, G.R., Bergamaschi, B.A., Fram, M.S., Fujii, R., Mopper, K., 2003. Evaluation of specific ultraviolet absorbance as an indicator of the chemical composition and reactivity of dissolved organic carbon. *Environ. Sci. Technol.* 37, 4702–4708.
- Widory, D., 2007. Nitrogen isotopes: tracers of origin and processes affecting PM₁₀ in the atmosphere of Paris. *Atmos. Environ.* 41, 2382–2390.
- Zappoli, S., Andracchio, A., Fuzzi, S., Facchini, M.C., Gelencser, A., Kiss, G., Krivacsy, Z., Molnar, A., Meszaros, E., Hansson, H.C., Rosman, K., Zebuhr, Y., 1999. Inorganic, organic and macromolecular components of fine aerosol in different areas of Europe in relation to their water solubility. *Atmos. Environ.* 33, 2733–2743.
- Zsolnay, A., 2003. Dissolved organic matter: artefacts, definitions, and functions. *Geoderma* 113, 187–209.
- Zsolnay, A., Baigar, E., Jimenez, M., Steinweg, B., Saccomandi, F., 1998. Differentiating with fluorescence spectroscopy the sources of dissolved organic matter in soils subjected to drying. *Chemosphere* 38 (1), 45–50.